# Observation of fine interference structures at total internal reflection of focused light beams

Valery N. Konopsky* and Elena V. Alieva
*Institute of Spectroscopy, Russian Academy of Sciences, Fizicheskaya 5, Troitsk, Moscow region 142190, Russia*
(Received 14 July 2012; published 5 December 2012)

We report the experimental observation of fine interference patterns in a reflection profile of a focused laser beam when it undergoes total internal reflection from a dielectric interface near its critical angle. In addition, we show that similar interference structures routinely appear in the reflection profile when long-range optical surface waves are excited at the plane interface by the focused laser beam. In both cases these interference patterns do not appear at all if the incident beam may be reckoned as a plane wave, that is, when the waist of the focused beam is much larger than the Goos-Hänchen shift or the surface wave propagation length correspondingly. A modified formula for the Goos-Hänchen shift is presented, and it is shown that a maximum value of the shift may reach several tens of microns for wide beams.

DOI: 10.1103/PhysRevA.86.063807 PACS number(s): 42.25.Gy, 42.70.Qs, 78.68.+m

The reflection of light from a planar interface is one of the most familiar and simple optical phenomena. For a perfect plane wave it is well described by reflection coefficients given by Fresnel formulas. However, in the real world, there is no such thing as perfect plane waves, i.e., infinite plane waves without divergence and incident on an infinite surface. Any real, confined beam of light contains an angular spectrum of plane waves and may be represented as a sum of plane waves propagating in slightly different directions. Some fine effects in specular reflection, originating from this fact, such as angular deviation of a reflected light beam, have attracted more attention in recent years [1–3]. In the present paper we describe the appearance of an interference pattern at total internal reflection near the critical angle.

Total internal reflection (TIR) is a well-known effect in optics that has many important applications. One of the classical applications of the TIR effect is Abbe refractometry, where measurement of the critical angle is used to derive the refractive index (RI) of a sample under investigation [4–6]. Here we show that despite the very long history and numerous papers published 140 years since the first Abbe work [7], some fine features of this effect remain to be elucidated.

A sketch of our experimental setup is shown in Fig. 1: A parallel light beam (with diameter $D = 10$ mm) from a fiber-coupled laser diode ($\lambda = 658$ nm) is focused on a base of a BK-7 prism by a cylindrical lens with a focal length $f = 40$ mm. The intensity distribution of the reflected light beam is detected by a CMOS matrix (with pixel pitch 8 $\mu$m) placed 80 mm away from the prism base. A flow cell is filled with water, in which the TIR occurs.

The measured data are displayed in Fig. 2(a), where $p$-polarization data is presented by red (gray) open dots, while $s$-polarization is shown by blue (dark gray) plus signs. The interference pattern is clearly seen for both polarizations in the region of the TIR (at $\theta > 61.5$ grad). We have routinely observed the same interference structures not only at TIR from water, but also at TIR from other liquids (e.g., ethanol) and at TIR from air (without a fluid cell at all). Other laser sources with narrow linewidth (frequency-stabilized He-Ne laser, for example) produce similar interference structures as well.

*konopsky@gmail.com; valery.konopsky.com

Theoretical simulations for TIR of the focused light beam from the interface between glass and water are shown in Fig. 2(b), where the red (gray) solid curve presents $p$-polarization, while the blue (dark gray) solid curve presents $s$-polarization. Details regarding theoretical calculations of reflection of the focused light beam from plane interface beam may be found in the Appendix. One can see that the measured data in Fig. 2(a) are in good agreement with theoretical simulations in Fig. 2(b).

Strong focusing of the laser beam is crucial for observing this interference pattern. This interference cannot be theoretically predicted from Fresnel-based calculations where the incident field is approximated as an infinite flat front, while the accurate theoretical simulations (reported in the Appendix), which take into account the focusing of the laser beam, reproduce this fringe pattern well.

To obtain additional physical insight into this effect it may be useful to recall that a similar fringe pattern was experimentally observed at the reflection of a focused beam from an interface supporting long-range propagating surface waves, such as long-range surface plasmon-polaritons [8–10] and photonic crystal surface waves (PCSW's) [11]. PCSW's are excitations of optical modes that can exist on the external surface of a photonic crystal in its band-gap region. Sometimes these PCSW's are also called Bloch surface waves [12] or optical Tamm states [13]. To illustrate this, Fig. 3 shows the reflection profile of an $s$-polarized focused laser beam from a seven-layer structure, supporting an $s$-polarized PCSW. The experimental setup is the same as in Fig. 1, and the only difference is that the seven-layer structure is deposited on the base of the prism [14,15].

In this case the fringe pattern is observed on the larger-angle side of the resonance dip (e.g., of a surface plasmon resonance dip). Theoretical simulations presented in Refs. [8,10,16] describe this interference pattern near the resonance dip rather well. Physical insight into the origin of this fringe pattern was proposed in Refs. [8,10]: this fringe pattern near the dip is the result of the interference between a divergent reflected Gaussian wave and a more flat leaky surface wave that is back-coupled into the prism from the interface. The waist difference of these two interfering beams leads to the difference in Rayleigh ranges and to the difference in wave-front curvatures of these beams at some distance. Intersections of two constant

 

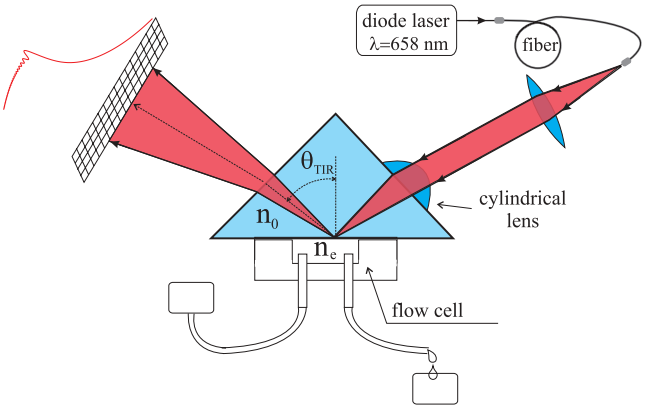


FIG. 1. (Color online) A sketch of the experimental setup.

phase fronts, which have different front curvatures, produce the interference pattern.

We suppose that a similar physical explanation may hold in the case of TIR from the interface between a glass prism and a dielectric (e.g., water, air, etc.). Despite the fact that this interface does not support long-range propagated surface waves, the Goos-Hänchen (GH) shift [17] takes place at the interface, the value of which is maximized exactly at the critical angle of TIR.

There are two main approaches to derive the Goos-Hänchen shift: the Artmanns method [18], where the GH shift is proportional to the first derivative of the phase of the reflectance, and Renards method [19], where energy flux along the interface is calculated. Near the critical angle of TIR, both methods give approximately the same value for the shift:

$$L_s \simeq \frac{1}{\pi}\frac{n_e}{n_0}\frac{\lambda}{\sqrt{\rho^2 - n_e^2}}, \tag{1}$$

where $L_s$ is GH shift for $s$-polarization; $n_0$ and $n_e$ are refractive indexes of the prism and the external medium, respectively; while $\rho = n_0 \sin(\theta_0)$ is an angle variable (numerical aperture). For $p$-polarization, $L_p \simeq (n_0/n_e)^2 L_s$.

The question is how large the GH shift may be in the immediate vicinity of the critical angle of TIR. Let us consider a parallel light beam, with a diameter $D$, incident on the interface at an angle $\rho$. Exactly at the critical angle (i.e., at $\rho = n_e$), the GH shift (1) is singula; however, even theoretically one

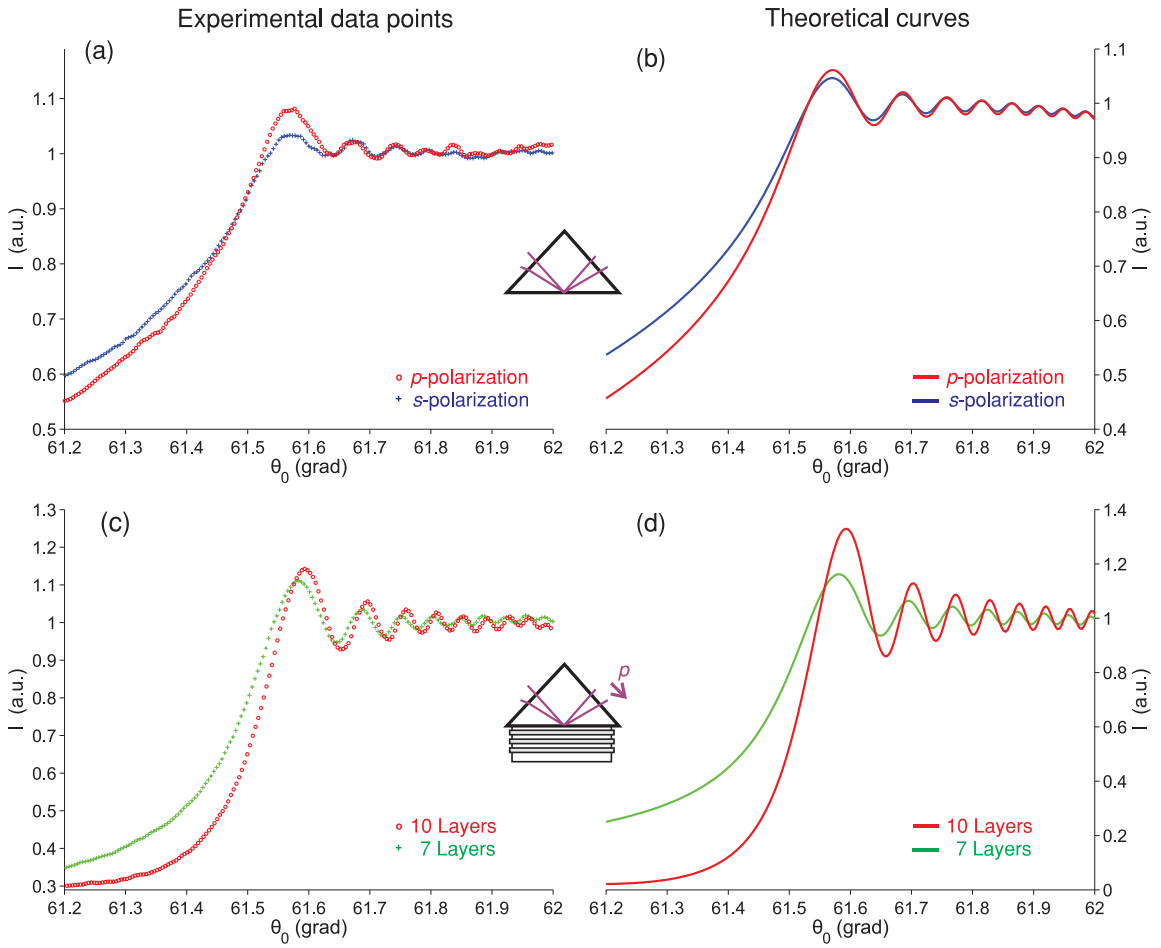


FIG. 2. (Color online) Reflection profiles near the critical angle: experimental data (dotted lines in the left column) and theoretical calculations (solid curves in the right column). Data of TIR from the bare prism for $p$- and $s$-polarization are shown in (a) (measurements) and (b) (simulations), while TIR data from the multilayer coated prism for the $p$-polarized beam are shown in (c) (measurements) and (d) (simulations).

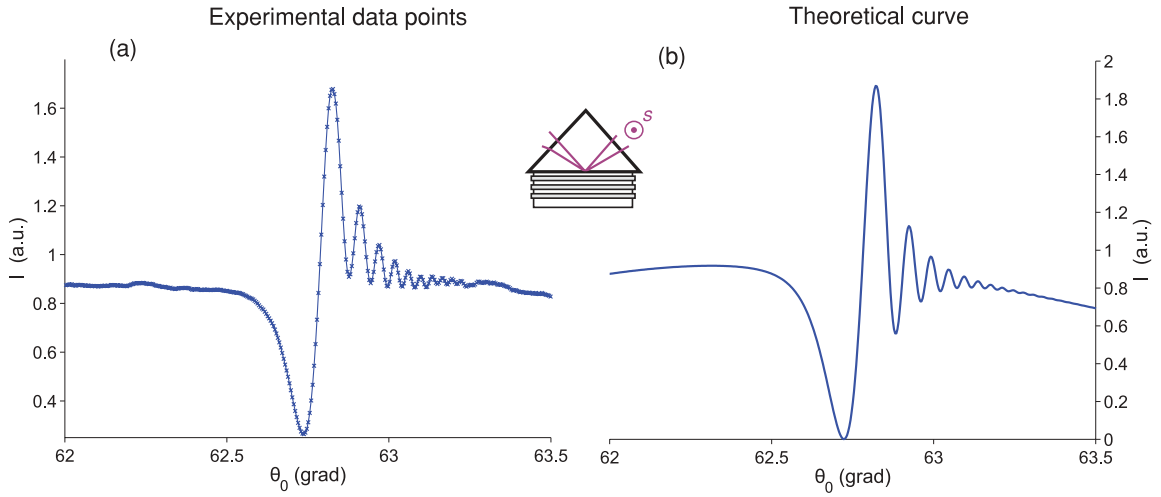


FIG. 3. (Color online) The reflection profile of $s$-polarized focused laser beam from the multilayer coated prism, supporting the $s$-polarized surface mode. Experimental data (a) and theoretical calculations (b).

cannot locate the point of critical angle with precision higher than a natural divergence of an optical beam, which depends on the beam diameter and wavelength. In other words, each photon in the beam has an angular uncertainty (or an angular smearing) on the order of $\delta\theta_0 \simeq \lambda/(n_0 D)$, and it is a direct consequence of the uncertainty principle ($\delta x \delta p_x \sim h$). To take into account the averaging of the GH shift due to the natural angular smearing of photons, we set

$$\langle L_s \rangle = \frac{1}{\delta\rho}\int_{\rho}^{\rho+\delta\rho} L_s d\rho = \frac{n_e\lambda}{\pi n_0 \delta\rho}\ln\left(\frac{\rho+\delta\rho+\sqrt{(\rho+\delta\rho)^2-n_e^2}}{\rho+\sqrt{\rho^2-n_e^2}}\right), \quad (2)$$

where $\delta\rho = n_0\cos(\theta_0)\delta\theta_0 \simeq \lambda\cos(\theta_0)/D = \lambda(1-\rho^2/n_0^2)^{1/2}/D$. For $p$-polarization, $\langle L_p\rangle \simeq (n_0/n_e)^2\langle L_s\rangle$ as usual.

Our modified equation for the GH shift of a parallel laser beam (2) has no singularities at $\rho = n_e$; however, it reaches its maximal value at this point:

$$\langle L_s\rangle_{\max} = \frac{\lambda}{\pi n_0}\sqrt{\frac{2n_e}{\delta\rho}} = \frac{\sqrt{\lambda D}}{\pi n_0}\sqrt{\frac{2n_e}{\cos(\theta_0)}}. \quad (3)$$

In Fig. 4 the angular dependence of the GH shifts are shown near the critical angle of TIR at the glass-water interface ($\rho_{\mathrm{TIR}} = n_e = 1.3304$). Substituting our values into Eq. (3), it may be shown that the largest theoretically possible GH shifts (at the glass-water interface) are equal to $\langle L_p\rangle_{\max} \simeq 51.7\,\mu$m for $p$-polarization and $\langle L_s\rangle_{\max} \simeq 39.9\,\mu$m for $s$-polarization, while for a standard laser beam with diameter $D \simeq 1$ mm these values are only 20.2 and 8.8 $\mu$m, respectively (at the glass-air interface; $n_e = 1$). As far as we know, the largest GH shift experimentally measured so far is 23.4 $\mu$m (for $p$-polarization at a glass-air interface with a 7-mm-wide beam) [20].

Hence, the maximal GH shift of a parallel beam (with $D \simeq 10$ mm) is much larger than the waist of the focused laser beam. In our experiments the focal waist at the interface is $f\lambda/[D\cos(\theta_0)n_0] \sim 4\,\mu$m, which is much less than $\langle L_p\rangle_{\max}$ and $\langle L_s\rangle_{\max}$ given above. Therefore, counting the focal intensity at the surface as a sum of plane waves and considering how each of these plane waves undergoes the GH shift, it seems reasonable that the physical explanation for appearance of the interference pattern near the TIR angle may be analogous to one for fringes near the resonance dip of long-range surface waves: The angular spectrum of the focused laser beam contains both the TIR angle (plus vicinity angles), where the GH shift is maximized, and angles far from TIR, where the GH shift is negligible. The latter angles generate a reflected divergent beam with the small waist, determined by the cylindrical lens in the incident beam, while the former angles generate a less divergent outcoming beam with a larger waist, determined by the GH shift. The interference pattern appears as a result of intersections of phase fronts of these beams with different curvatures—as described above for long-range surface waves.

To give an additional proof that the observed interference pattern is connected with the long-range energy flux along the interface, we perform experiments where this energy flux is enhanced by a multilayer deposited on the prism base. We used 7- and 10-layer 1D photonic crystal structures for this purpose.

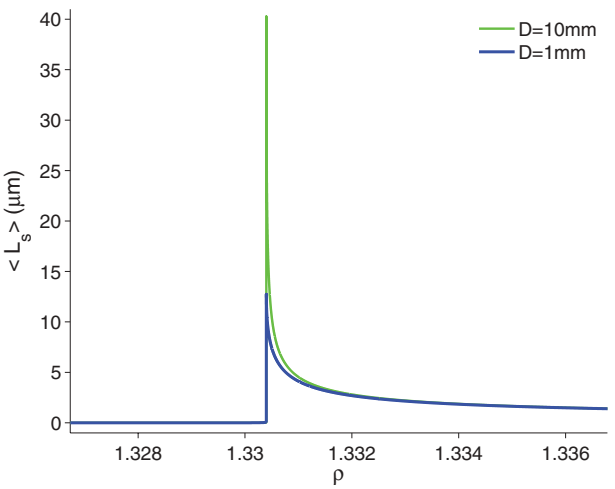


FIG. 4. (Color online) The Goos-Hänchen shift near the critical angle at the glass-water interface according to Eq. (2) for 1- and 10-mm-wide laser beams.

In these structures a $p$-polarized PCSW exists; however, for this number of layers, it is extremely lossy due to leakage into the prism. As a result, the dispersion curve of this $p$-polarized mode is extremely wide and no resonance dip at $\lambda = 658$ nm is present in the reflection profile (about 20 layers are needed to build a "mature" $p$-polarized mode, appearing at $\lambda < 658$ nm). Nevertheless, these 7- and 10-layer structures enhance the energy flux along the interface near the critical angle to some degree.

The results are shown in Fig. 2(c) and 2(d), where the measured experimental points are shown in (c) as open red (gray) dots for 10-layers and as green (light gray) cross signs for 7-layers, while in (d) the theoretical simulations are shown (see Appendix for details). Theoretical curves in Fig. 2(d) agree well with experimental data. One can see that the interference pattern becomes more pronounced with enhancement of energy flux along the surface. A small reflection coefficient below the critical angle is the result of a destructive interference between the reflected wave and the lossy surface wave that reradiates back to the prism with the corresponding rotation of its phase.

In conclusion, it must be pointed out that the interference patterns, appearing near the critical angle of TIR and near the resonance dip of long-range surface waves, not only have academic interest, but are also very important and useful for sensing applications [21,22]. The reason is that the increase in number of points with large values of the first derivative near the dip and near the critical angle leads to an increase in sensitivity to changes in their position.

This work was partially supported by the Science and Technology Cooperation Programme Switzerland–Russia.

## APPENDIX: THEORETICAL SIMULATION OF THE FOCUSED GAUSSIAN BEAM REFLECTION FROM A PLANE INTERFACE

Here we calculate the reflection profile of a focused Gaussian beam when it is reflected off an interface with reflection coefficient $R$. An explanatory scheme and axes of coordinates are presented in Fig. 5.

Since we focus our beam by the cylindrical lens, we will use a two-dimensional presentation of the Gaussian beam, depending on two spatial coordinates $x'$ and $z'$ (the $y'$ coordinate is omitted):

$$E(x',z') = E_0 \frac{\omega_0}{\omega(z')} \exp\left(-\frac{x'^2}{\omega^2(z')}\right) \times \exp\left[-ik\left(z' + \frac{x'^2}{2R(z')}\right) + i\varphi(z')\right], \quad \text{(A1)}$$

where

$$\omega(z') = \omega_0 \sqrt{1 + \left(\frac{z'}{z_0}\right)^2} \quad \text{(A2)}$$

is the beam radius and $\omega_0$ is the beam waist,

$$R(z') = z'\left[1 + \left(\frac{z'}{z_0}\right)^2\right] \quad \text{(A3)}$$

is the radius of curvature of the wave fronts comprising the beam,

$$k = \frac{2\pi}{\lambda} n_0 \quad \text{(A4)}$$

is the wave vector, and

$$\varphi(z') = \arctan\left(\frac{z'}{z_0}\right) \quad \text{(A5)}$$

is the longitudinal phase delay of the beam. The Rayleigh range of the beam $z_0$, in the above equations, equals

$$z_0 = \pi \frac{\omega_0^2}{\lambda} n_0 \,. \quad \text{(A6)}$$

We will assume that the beam is focused at the interface ($z' \sim 0$) and that the beam focus is larger than the wavelength ($\omega_0 > \lambda$). With these assumptions Eqs. (A2) and (A5) may be simplified to

$$\omega(z') \simeq \omega_0\left[1 + \frac{1}{2}\left(\frac{z'}{z_0}\right)^2\right], \quad \text{(A7)}$$

$$\varphi(z') \simeq \left(\frac{z'}{z_0}\right). \quad \text{(A8)}$$

After a coordinate system transform (rotation by angle $\theta_0$),

$$\begin{aligned} x' &= x\cos(\theta_0) - z\sin(\theta_0) \\ z' &= x\sin(\theta_0) + z\cos(\theta_0), \end{aligned} \quad \text{(A9)}$$

we make the Fourier transformation of our beam at the interface (i.e., at $z = 0$):

$$E(k_x) = \int_{-\infty}^{\infty} E(x,0)\exp(ik_x x)dx. \quad \text{(A10)}$$

This transformation from spatial to angular coordinates permits us to use Fresnel formulas for each plane wave in the angular presentation of the Gaussian beam.

It is very convenient to use a numerical aperture $\rho = n_j \sin(\theta_j)$ as a unified angle variable in a multilayer, instead of angles $\theta_j$ in each $j$th layer, and hereafter, we will do so. After appropriate transforms of variables

$$\begin{aligned} \theta_0 &= \arcsin(\rho_0/n_0) \\ k_x &= 2\pi\rho/\lambda, \end{aligned} \quad \text{(A11)}$$

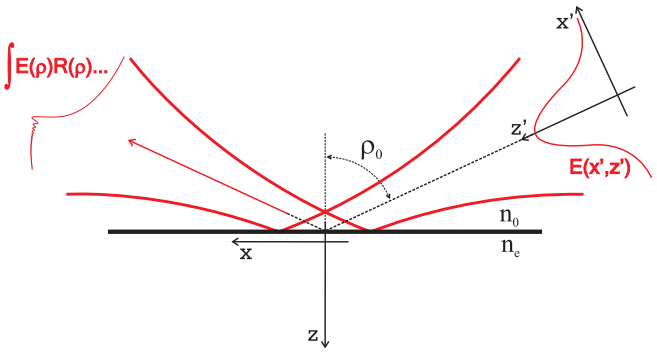


FIG. 5. (Color online) The axes of coordinates and the explanatory scheme for calculations.

the result of integration in (A10) has the form

$$E(\rho) \simeq \frac{E_0 n_0 \omega_0 \sqrt{\pi}}{\sqrt{n_0^2 - \rho_0^2}} \exp\left(-\frac{(\rho-\rho_0)^2}{(n_0^2-\rho_0^2)} \frac{n_0^2 \omega_0^2 \pi^2}{\lambda^2}\right), \quad \text{(A12)}$$

where $\rho_0$ is the angular coordinate of the beam axes.

Now, to obtain the required profile of the reflected beam, we make an inverse Fourier transformation after multiplying each plane wave component by the complex reflection coefficient $R$:

$$E(x,z) \simeq \int_0^{n_0} E(\rho) R(\rho) \exp\left[-i\frac{2\pi}{\lambda}\left(x\rho + z\sqrt{n_0^2-\rho^2}\right)\right] d\rho. \quad \text{(A13)}$$

This is the final result of this section. As a rule, a numerical integration is needed in this final step. The reflection coefficient $R$ as a function of $\rho$ may be found, for example, from Fresnel's formula written in impedance terms. For the interface between semi-infinite media $_{(0)}$ and $_{(e)}$, it has a very simple form:

$$R = \frac{Z_{(e)} - Z_{(0)}}{Z_{(e)} + Z_{(0)}}, \quad \text{(A14)}$$

where $Z_{(j)}$ is the normal impedance of medium $j$, given by (A15) or (A16). The use of $R$ and $Z$ (without subscripts $s$ or $p$) means that the equation holds for both polarizations when the corresponding impedances $Z_s$ or $Z_p$ are inserted.

The impedances for $s$- and $p$-polarizations have the following forms as functions of $\rho$:

$$Z_{s(j)} = \frac{1}{n_j \cos(\theta_j)} = \frac{1}{n_j\sqrt{1-(\rho/n_j)^2}}, \quad \text{(A15)}$$

$$Z_{p(j)} = \frac{\cos(\theta_j)}{n_j} = \frac{\sqrt{1-(\rho/n_j)^2}}{n_j}. \quad \text{(A16)}$$

For reflection from a multilayer Eq. (A14) may also be used, where an apparent input impedance $Z_{(j)}^{\text{into}}$ is inserted instead of $Z_{(e)}$ (see, for example, Ref. [23] for more details). The apparent input impedance $Z_{(j)}^{\text{into}}$ of a semi-infinite external medium $_{(e)}$ and layers from $N$ to $j$ may be calculated by the following recursion relation:

$$Z_{(j)}^{\text{into}} = Z_{(j)} \frac{Z_{(j+1)}^{\text{into}} - i Z_{(j)} \tan(\alpha_j)}{Z_{(j)} - i Z_{(j+1)}^{\text{into}} \tan(\alpha_j)}, \quad \text{(A17)}$$

where $\alpha_j = k_{z(j)} d_j = (2\pi/\lambda) n_j \cos(\theta_j) d_j$; $j = N, N-1, \ldots, 2, 1$ and $Z_{(N+1)}^{\text{into}} = Z_{(N+1)} = Z_{(e)}$, $n_{N+1} = n_e$ while $d_{N+1} = d_e = 0$ by definition.

We used this recursion relation to calculate $R(\rho)$ for our 7- and 10-layer structures and then numerically calculated the integral (A13). The results of the calculations are shown as solid curves in corresponding figures in the article. One can see that the interference structures are reproduced well in the theoretical curves obtained by this method.

Finally, it is interesting to note that it was Isaac Newton who first expressed suspicion that total internal reflection does not take place at the geometrical interface between the two media. According to his treatment of the nature of light as a beam of particles, the path of these particles at TIR should be a parabola with a vertex located in the less-dense medium that results in an offset between the incident and reflected points. Hence, the experimental detection of the GH shift would be considered by Newton as confirmation of his model of particles of light, which are attracted to the denser medium. However, even in this effect, a wave nature of light shows itself through an interference pattern, appearing after simple focusing at the TIR angle.


[1] G. Nimtz, Nat. Photonics **3**, 319 (2009).

[2] M. Merano, A. Aiello, M. P. van Exter, and J. P. Woerdman, Nat. Photonics **3**, 337 (2009).

[3] F. Krayzel, R. Pollès, A. Moreau, M. Mihailovic, and G. Granet, J. Eur. Opt. Soc. RP **5**, 10025 (2010).

[4] P. Herrmann, Appl. Opt. **19**, 3261 (1980).

[5] G. Meeten and A. North, Meas. Sci. Technol. **6**, 214 (1995).

[6] Q. Song, C. Ku, C. Zhang, R. Gross, R. Birge, and R. Michalak, J. Opt. Soc. Am. B **12**, 797 (1995).

[7] E. Abbe, in *Jenaische Zeitschrift für Naturwissenschaft* (Mauke's Verlag, Jena, Germany, 1874), Vol. 8, pp. 96–174.

[8] V. N. Konopsky and E. V. Alieva, Phys. Rev. Lett. **97**, 253904 (2006).

[9] H. J. Simon, R. V. Andaloro, and R. T. Deck, Opt. Lett. **32**, 1590 (2007).

[10] V. N. Konopsky and E. V. Alieva, Opt. Lett. **34**, 479 (2009).

[11] V. N. Konopsky and E. V. Alieva, Anal. Chem. **79**, 4729 (2007).

[12] E. Descrovi, T. Sfez, M. Quaglio, D. Brunazzo, L. Dominici, F. Michelotti, H. P. Herzig, O. J. F. Martin, and F. Giorgis, Nano Lett. **10**, 2087 (2010).

[13] T. Goto, A. V. Baryshev, M. Inoue, A. V. Dorofeenko, A. M. Merzlikin, A. P. Vinogradov, A. A. Lisyansky, and A. B. Granovsky, Phys. Rev. B **79**, 125103 (2009).

[14] Two photonic crystal structures were used in these experiments: a 7-layer structure and a 10-layer structure. The first multilayer had a structure: prism/$(LH)^3L'$/water, while the second had a structure: prism/$H(LH)^4L'$/water. In this notation $H$ is a $Ta_2O_5$ layer with thickness 111.5 nm, $L$ is a $SiO_2$ layer with thickness 183.5 nm, and $L'$ is a $SiO_2$ layer with thickness 346.2 nm.

[15] The $Ta_2O_5/SiO_2$ multilayer was deposited by magnetron sputtering. The prism was made from BK-7 glass. The refraction indices of the prism, $SiO_2$, $Ta_2O_5$ layers, and water at $\lambda =$ 658 nm were $n_0 = 1.514$, $n_1 = 1.47$, $n_2 = 2.06$, and $n_e =$ 1.3304, respectively.

[16] R. V. Andaloro, R. T. Deck, and H. J. Simon, J. Opt. Soc. Am. B **22**, 1512 (2005).

[17] F. Goos and H. Hänchen, Ann. Physik **436**, 333 (1947).

[18] K. Artmann, Ann. Physik **437**, 87 (1948).

[19] R. H. Renard, J. Opt. Soc. Am. **54**, 1190 (1964).

[20] H. G. L. Schwefel, W. Köhler, Z. H. Lu, J. Fan, and L. J. Wang, Opt. Lett. **33**, 794 (2008).

[21] V. N. Konopsky and E. V. Alieva, Biosens. Bioelectron. **25**, 1212 (2010).

[22] www.pcbiosensors.com.

[23] V. N. Konopsky, New J. Phys. **12**, 093006 (2010).